Chemical Engineering Science 153 (2016) 155–164

Contents lists available at ScienceDirect

Chemical Engineering Science

journal homepage: www.elsevier.com/locate/ces

Particle tracking using micro bubbles in bubbly flows

T. Ziegenhein*, M. Garcon, D. Lucas

Helmholtz-Zentrum Dresden-Rossendorf e.V., 01314 Dresden, Germany

HIGHLIGHTS

- Non-intrusive liquid velocity measurements in bubbly flows.
- Particle tracking velocimetry (PTV) for high void fractions.
- Sampling bias in bubbly flows for PTV is described.
- Very simple, cheap and robust measuring method.
- Particle tracking velocimetry is compared to particle image velocimetry.

ARTICLE INFO

Article history:
Received 24 November 2015
Received in revised form
13 July 2016
Accepted 20 July 2016
Available online 21 July 2016

Keywords:
Bubble tracking velocimetry
Sampling bias
Multiphase flow
Particle tracking velocimetry
Volume illumination
Particle image velocimetry

ABSTRACT

Micro bubbles do not contaminate multiphase flows like additional tracer particles so that the velocity in such can be determined completely non-intrusive by tracking them. They are, however, often larger as conventional tracer particles and have a significantly different density than the surrounding fluid. The usability of micro bubbles as tracers in bubbly flows, particularly in buoyancy driven flows, is investigated in this work. The results are compared to particle image velocimetry measurements using PMMA tracer particles. In combination with the used volume illumination, a simple, robust and reliable measuring technique is discussed, which is deployable for complex problems like photo bioreactors or submerged oceanic multiphase flows.

Averaged liquid velocities as well as basic turbulence parameters are determined in a rectangular bubble column for different gas volume flow rates. High flow rates are good manageable due to the volume illumination whereas the PIV measurements using a light sheet are approaching to their limits. The general sampling bias in multiphase flows found recently for PIV measurements is also present for particle tracking methods; a hold processor that waits a time depending on the distribution of the particle information over the measuring area gives reasonable results.

1. Introduction

The velocity field in multiphase flows is measured in order to get a better understanding of the underlying processes. For this purpose, measuring methods that were developed for single-phase flow are used, e.g. the laser Doppler anemometry (LDA), hot film anemometry (HFA), particle-tracking velocimetry (PTV) or the particle image velocimetry (PIV). Except of HFA, tracer particles have to be added to the flow.

In single-phase flows, such tracer particles do not disturb the flow, whereas in multiphase flows these particles often tend to accumulate at the interfaces so that the flow could be affected. In addition, tracer particles contaminate the facility in general, which might disturb chemical as well as biological processes. Besides, the seeding of particles might be problematic for some applications, e.g. for oceanographic measurements. To overcome such problems naturally occurring micro bubbles can be used as tracer particles.

Tracking micro bubbles to determine the velocity of the continuous phase is not extensively investigated yet. Nevertheless, some applications can be found in literature, e.g. in breaking waves (Ryu, et al., 2005), behind propellers (Graff, et al., 2008), around dolphin (Fish, et al., 2014) s or in horizontal channels (Murai, et al., 2006). Noteworthy, micro bubbles can also be explicitly generated for particle tracking as for example shown by Ishikawa et al. (2009).

In the present work, particle-tracking velocimetry with micro bubbles (BTV) in bubbly flows is investigated in a rectangular tabletop bubble column. The results obtained by tracking micro bubbles in the range of 150–300 μm are compared to PIV

* Corresponding author.
E-mail address: t.ziegenhein@hzdr.de (T. Ziegenhein).

http://dx.doi.org/10.1016/j.ces.2016.07.024
0009-2509/

measurements. For simplicity as well as to investigate higher void fractions, a volume illumination is used for the BTV measurements. A two dimensional measuring plane is obtained from the illuminated volume by using a narrow depth of field in combination with an edge filter technique.

The presence of the larger bubbles disturbs the liquid velocity measurements in general so that a sampling bias occurs. This sampling bias is described by Ziegenhein and Lucas (2016) for PIV measurements, which is also present for the BTV measurements. A window averaging method is used to overcome this error.

Overall, a reliable measurement technique is described which is very simple, cheap and flexible deployable. Thus, reliable measurements might be realized in new fields of application to gain a better understanding of such. Moreover, a larger quantity of high quality measurements in a wide field of multiphase applications, which are vitally needed for CFD validation (Ziegenhein, et al., 2015; Ma, et al., 2015; Masood, et al., 2014), can be realized.

2. Experimental setup

The bubble column shown in Fig. 1 was used for the measurements. The bubble column is 50 mm deep and 250 mm width, the water level without gas was 800 mm. The liquid velocity was measured 200 mm above the ground plate along the centerline. The sparger, which is installed level with the ground plate, consists of eight needles with an inner diameter of 1.5 mm.

A 200-Watt LED light was placed behind the column. The images were recorded with a Redlake MotionPro High speed digital imaging system. A macro lens was used with a focal length of 300 mm.

Six different volume flows, which are given in Table 1, were investigated. The volume flow was measured and controlled with a mass flow controller. The volume flow of 0.375 l per min per needle was the smallest possible volume flow whereas 20 l per minute in total was the highest possible volume flow with the used mass flow controller.

Table 1
The different used gas volume flow rates at standard conditions.

Case number	Volume flow rate [liter/min]	Flow rate per needle [liter/min]
3	3	0.375
4	4	0.5
5	5	0.625
7	7	0.875
13	13	1.625
20	20	2.5

3. Particle tracking velocimetry

3.1. Micro bubble identification and tracking

The liquid velocity is determined by measuring the displacement of single micro bubbles. The measuring volume is illuminated completely; micro bubbles are identified on a two-dimensional plane by an edge filter technique in combination with a camera setup with a narrow depth of field. The technique is demonstrated in Fig. 2a) using test objects that are 1 mm displaced in depth. The field of maximum sharpness is situated between the fourth and the fifth object from the left. The blurring is increasing with increasing distance to the field of maximum sharpness. The edge-detecting algorithm (Canny, 1986) is applied on a); the normalized edge strength is shown along the red-white dotted line in picture b). In this context, only the edges of the squares are of interest so the borders of the objects are excluded from the diagram to constitute the method clearly. A hysteresis on the edge strength is applied so that the blurred edges are excluded. For the shown example, the hysteresis would cut out all edges with strength below 0.8. With a similar test set-up, the depth of field was calibrated to 2 mm.

The identification of bubbles in the plane of best sharpness is shown in Fig. 3. After the edges are identified, the strength of the edges is set to the modulus of the derivation of the image gray scale at this point. Two thresholds are used on the edge strength to distinguish strong, weak and not considered edges. Afterwards, if a weak edge touches a strong edge it becomes a strong edge itself, which is repeated until no weak edge touches a strong edge.

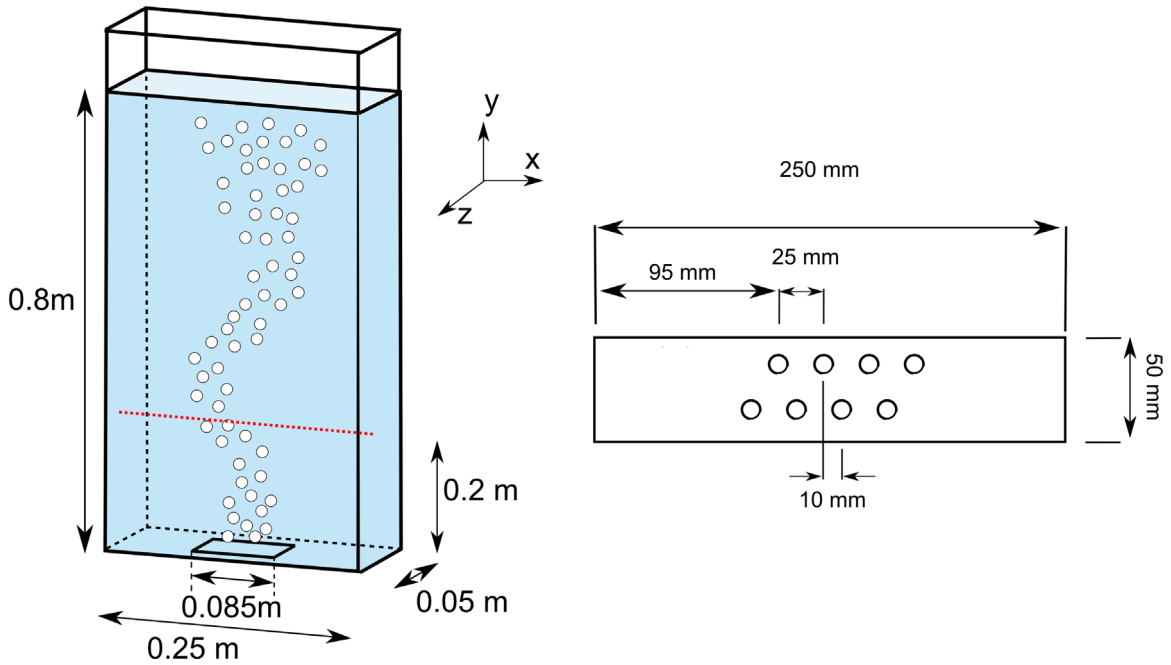

Fig. 1. Experimental setup. Left: Sketch of the facility, the measuring line is dotted. Right: The ground plate, the holes indicate the positions of the needle spargers.

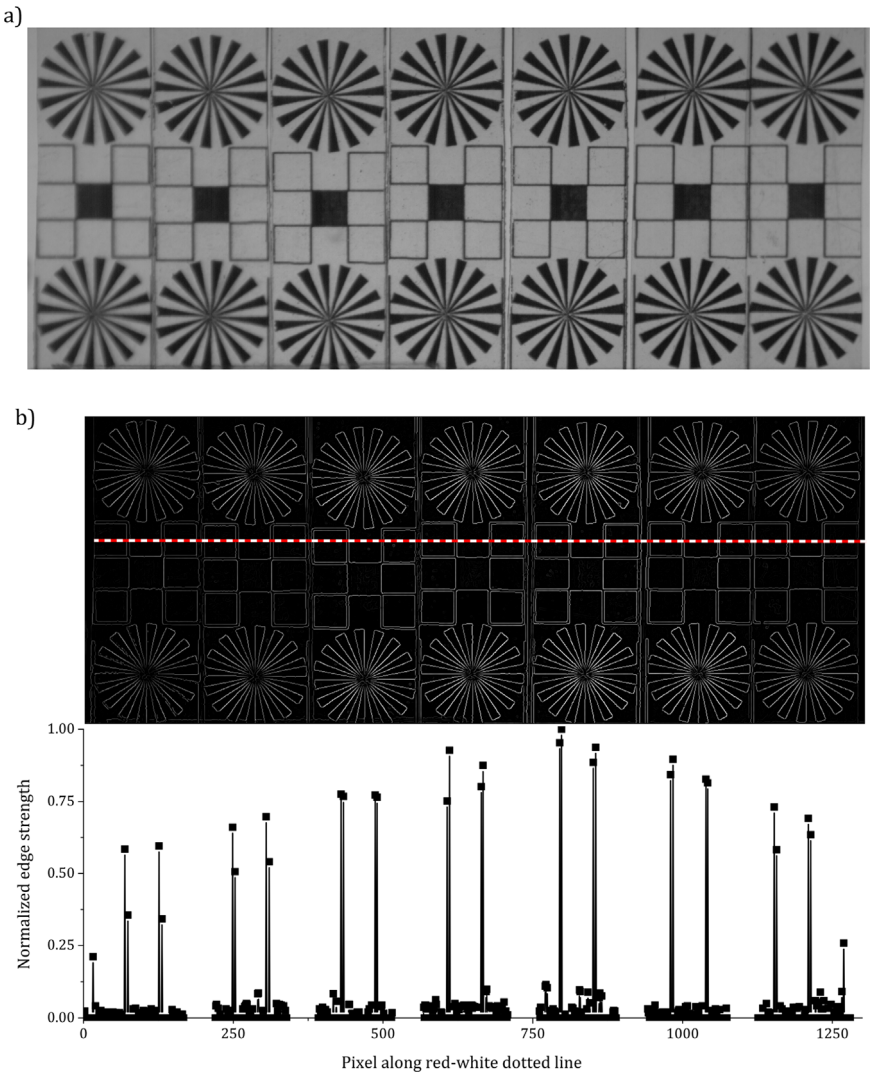

Fig. 2. Determining the depth of field by filtering the edge strength. The distance in depth between the test prints is 1 mm. a) Original picture, b) edge strength in gray shades and as graph along the dotted line.

Because of this hysteresis, the complete edge of a bubble in the measuring plane is obtained. Hereinafter, the boundaries of the bubbles have to be closed since the illumination is not always perfect as seen in Fig. 3.

The method is demonstrated in Fig. 4 under measurement conditions. The marked bubbles, which are in the maximum field of sharpness ± 1 mm, are used for tracking. The micro bubbles are spherical so that the centroid of the projected area is taken as the position. The micro bubbles are tracked four times (Feng, et al., 2011) by a pulsed camera every 1/1600 s. The velocity is calculated when the bubbles move its own radius, else, the position in the next picture of the four is used. If a bubble do not move its own radius during the four recorded pictures, the first and the last is used for tracking.

3.2. Stokes time and terminal velocity

The characteristic time scale of complex bubbly flows is not known so that the Stokes number cannot be used to characterize the capability of the micro bubbles to follow the flow. To get an idea, however, the results obtained with different micro bubble sizes are compared below. In addition, the characteristic particle time scale is used in order to compare the micro bubbles with tracers used in similar experiments, which is shown in Table 2. Taking the virtual mass into account (Calzavarini, et al., 2008), the characteristic particle time scale is calculated to

$$\tau_P = \frac{1}{12}\frac{d_P^2}{\nu}\frac{2\rho_P+\rho_F}{3\rho_f}. \tag{3-1}$$

In general, the time scale of the used micro bubbles is comparable to other methods. The time scale of the small micro bubbles is in the range of the PIV particles used by Deen et al. (2001). LDA particles, however, have a distinctly smaller time scale whereas the polystyrene particles used for Computer-Automated Radioactive Particle Tracking (Luo & Al-Dahhan, 2008) have a significantly larger time scale.

Micro bubbles are lighter than water so that the rising velocity has to be subtracted from the measured velocity. In the present work, the rising velocity is calculated by using the drag law of Bozzano & Dente.(2001).

3.3. Sampling bias

A sampling bias occurs if a not representative sample, in which some values are less likely included than others, is picked. If the liquid velocity is measured with BTV in bubbly flows such a sampling bias occurs, as shown by Ziegenhein and Lucas (2016) for PIV

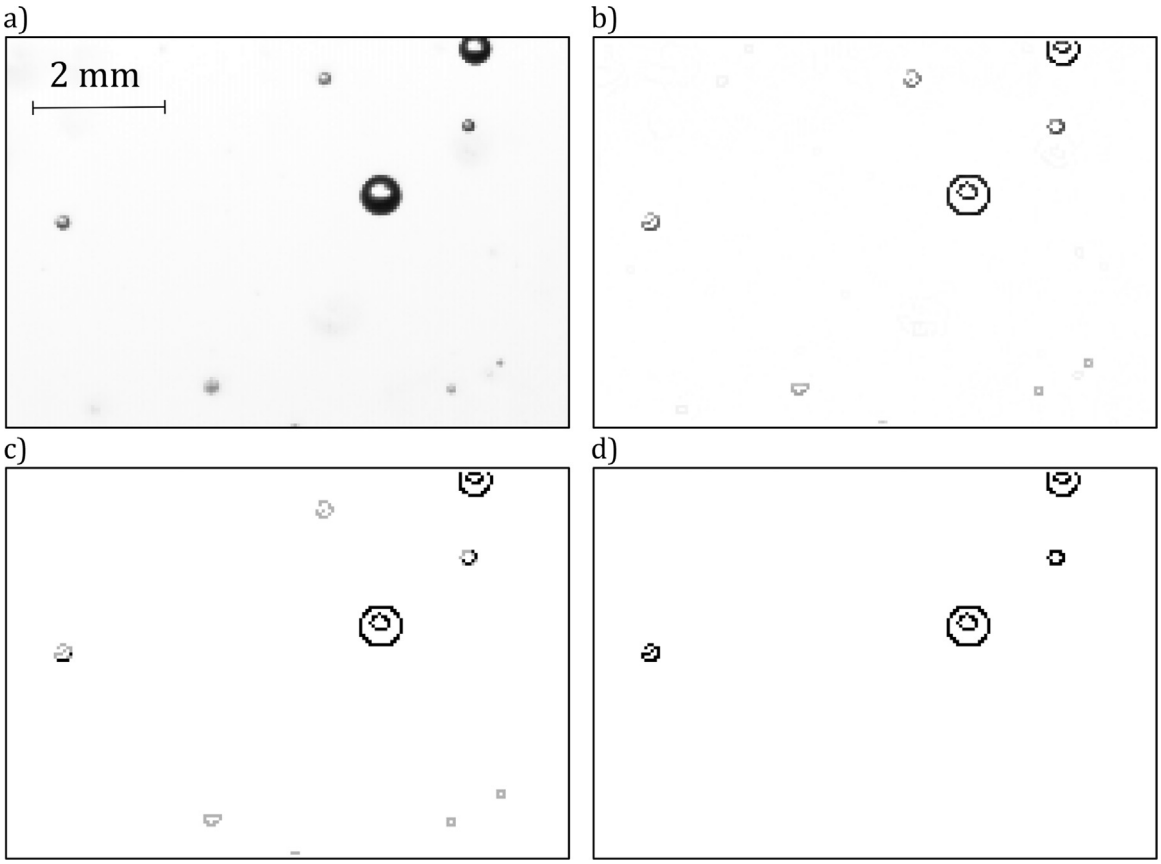

Fig. 3. Identifying bubbles in the plane of best sharpness using the Canny algorithm: a) Original image, b) edge Strength in gray scale, c) distinction in strong (black) and weak (gray) edges, d) result of the hysteresis.

Table 2
Characteristic particle time scale for different measurement techniques in bubbly flows.

Reference	Time scale τ_P	Particles	Method
Present work	100 μm: 0.3 ms 200 μm: 1.1 ms 300 μm: 2.5 ms	Bubbles d_P: 100–300 μm	Particle tracking
Deen et al. (2001)	0.21 ms	PMMA particles d_P: 50 μm	PIV
Juliá et al. (2007)	0.03 ms	Hole glass particles d_P: 20 μm	LDA
Luo & Al-Dahhan (2008)	53 ms	PS particles d_P: 800 μm	Computer-Automated Radioactive Particle Tracking (CARPT)

measurements. Bubbles that are passing the field of view hinder the view on the measuring plane. However, these large bubbles drive the flow so that higher velocities occur just when many of these bubbles are in the field of view. Since these velocities are less likely measured due to the large bubbles in the field of view, a sampling bias occurs. It should be noted, that the sampling bias is not caused by the bubbles inside the measuring plane, but by the bubbles out of it.

The sampling bias is demonstrated in Fig. 5. The count of the velocity information is low when the vertical velocity is high and vice versa. A window ensemble average in space and time is used in order to overcome this error, which is explained in detail by Ziegenhein and Lucas (2015). The window ensemble averaging in space is executed by dividing the measuring area in grid cells. For window

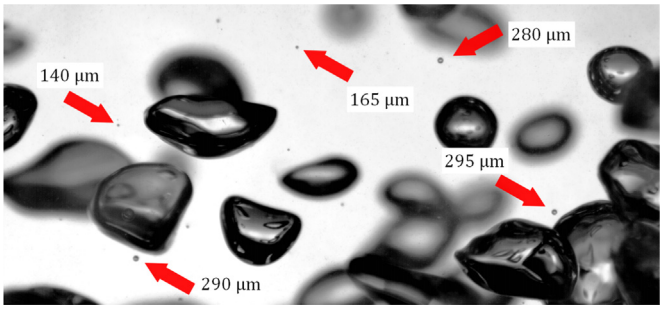

Fig. 4. Bubbles that are used for tracking in the field of maximum sharpness.

averaging in time, the time is waited until all grid cells contain at least one velocity track (hold time). After the hold time, all velocities that are collected in one grid cell are averaged. Thus, one value in each grid cell is obtained afterwards. After the complete measuring time, these averaged values are arithmetic averaged per grid cell.

If this hold processor is not used, distinct other results are obtained. In particular, the main component of the Reynolds stress tensor $v'v'$ would have been different in the center where most of the bubbles are situated.

4. Results

4.1. Size of the micro bubbles

The size of the micro bubbles that are used for particle tracking is not uniform and different at different positions as demonstrated

in Fig. 6. Hypothetically, if the smaller bubbles follow the flow better than the larger bubbles, locally different turbulence parameters are obtained. Therefore, it is essential to track bubbles in a range of size in which the capability to follow the flow is the same. Moreover, the general capability of the micro bubbles to follow the liquid flow fields is of interest to assess possible errors due to the larger size and smaller density of them compared to, for example, LDA or PIV particles.

The results that are obtained by tracking different micro bubble sizes are compared to each other in Fig. 7 for case 13. The vertical liquid velocity is similar for all bubble groups except for the group of 400–500 μm bubbles near the wall. Tracking larger micro bubbles, however, must not imply a larger vertical velocity due to the higher terminal velocity of them because the liquid velocity is corrected with this, as discussed above. Moreover, the results that are obtained by taking all bubbles (bubble group 150–500 μm) into account is not equal to the average of the results over all sub bubble groups because of the above described hold processor. In addition, the quantity of the tracked micro bubbles in the different bubble groups is not the same, but the quantity of the smallest group is sufficient to produce plausible results.

The normal Reynolds stress tensor component $v'v'$ (v is the vertical velocity) might indicate a different ability to follow the fluctuations of the flow for the different bubble sizes. Looking at b) in Fig. 7, a clear trend is seen; in the center, $v'v'$ is decreasing with increasing bubble size. The results obtained with the bubble groups ranging from 150 to 250 μm and from 200 to 300 μm, however, are almost equal.

In addition, the probability density function (PDF) of the fluctuations are shown in Fig. 7c and d; the larger and smaller micro bubbles have the same behavior in general. Although the quantity of the larger size group is smaller, the PDF is smoother. Particularly in picture c), the smaller size group contains 7600 tracks whereas the larger bubble size group only 6300 tracks. Despite this, the PDFs of the small bubbles and the large bubbles are similar, especially at the shoulders.

Overall, the results obtained using larger micro bubbles are different compared to the results using smaller micro bubbles. The trend of decreasing Reynolds stress tensor component $v'v'$ with increasing size might indicate a worse capability to follow the flow of these. However, the PDFs of the small and large bubbles are similar at high fluctuations. The results that are obtained using bubbles between 150 and 300 μm are similar for the present setup. Therefore, this bubble group is used for further investigations. Noteworthy, the good agreement between these results and the PIV results discussed in Section 4.3 might confirm that the chosen bubble size group is reasonable.

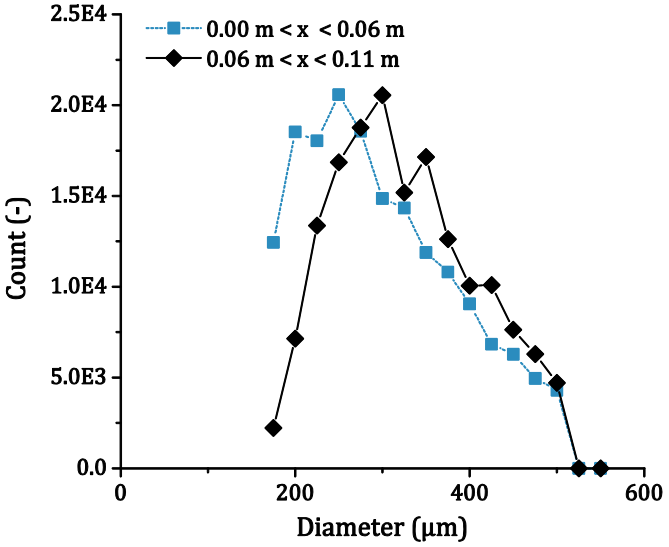

Fig. 6. Count of the tracked micro bubbles for case 13 in the wall region (0.00–0.06 m) and towards the center, which is at $x=0.125$ m.

4.2. Influence of the gas flow rates

The results for all cases are shown in Fig. 8. The progression of the vertical liquid velocity with increasing the gas volume flow rates is reasonable. As expected, the normal Reynolds stress tensor components $v'v'$ and $u'u'$ are increasing with increasing gas volume flow rates (u is the horizontal velocity). The graphs of $v'v'$ show a distinct peak between the wall and the center for all volume flows. In contrast, $u'u'$ is permanently increasing towards the center. This behavior is also described in other work using similar experimental setups, e.g. by Mudde et al. (1997) or Simiano et al. (2006). Since the flow regime is changing, the $v'v'$ and $u'u'$ values that are obtained for case 20 are distinctly higher than these for the other volume flows are. In case 20 all bubble sizes are pulled downwards in the recirculation zone so that the bubble column is completely filled with bubbles; whereas in case 13 bubble clusters are pulled downward occasionally and in case 7 only few bubbles. The possible outlier in the $u'u'$ graph obtained for case 20 at around $x=0.055$ m is discussed below.

4.3. Comparison with PIV

The results that are obtained with PIV are compared to those obtained with BTV. The PIV results are taken from our recently published work concerning the sampling bias (Ziegenhein and Lucas, 2015). The bubbly flow was seeded with 35–50 μm PMMA Rhodamine particles from microParticles GmbH in Berlin. All

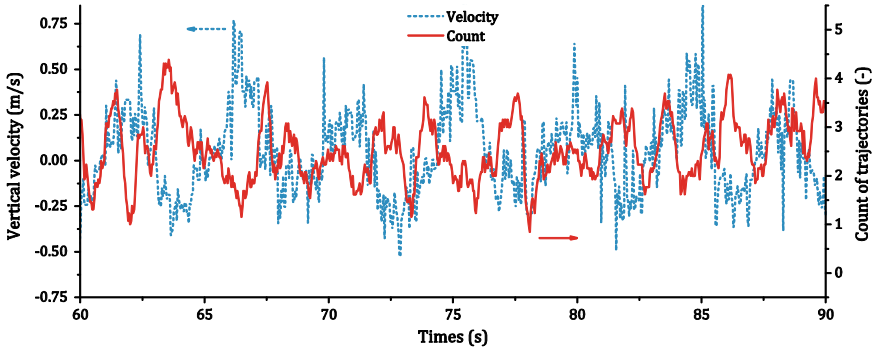

Fig. 5. Tracked vertical velocity (dashed line) and count of trajectories (continuous line) over time for Case 13 near the center at $x=0.1$ m.

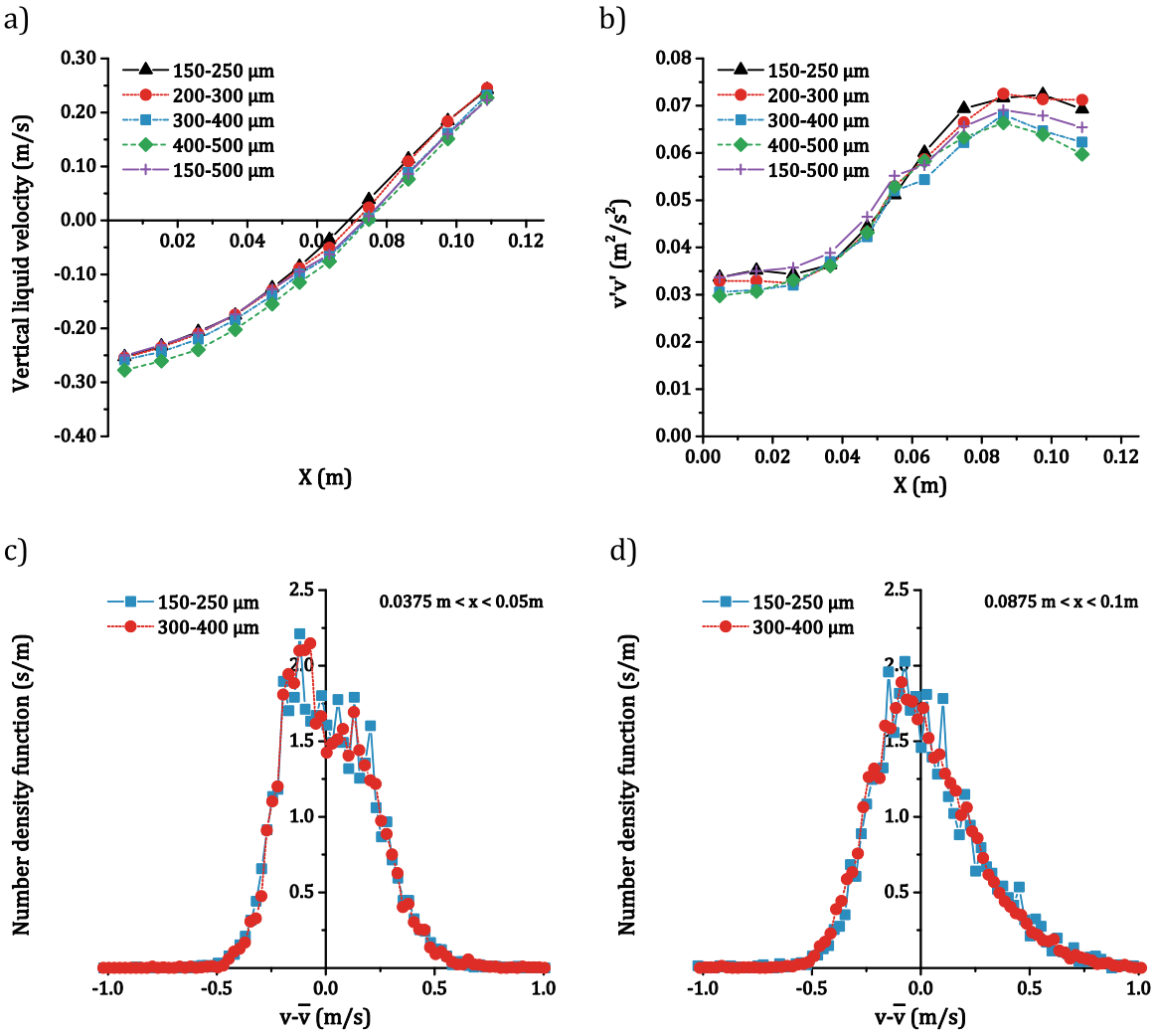

Fig. 7. Results that are obtained by tracking different bubble sizes for case 13, the profiles a) and b) are shown for only half of the column. a) The vertical liquid velocity v for the different bubble sizes, b) the normal Reynolds stress tensor component $v'v'$, c) the fluctuation probability function in 0.0375 m $< x <$ 0.05 m for two bubble groups, d) the fluctuation probability function in 0.0875 m $< x <$ 0.1 m for two bubble groups.

bubbles are cut out from the recorded PIV image by the use of an edge-detecting algorithm; every interrogation area that touches a bubble is cut out. The PIV and BTV experiments were executed successive on the same day. Thus, the same fluid and the same concentration of PIV particles were used for all experiments.

The recording time for the PIV measurements was 10 min per case. A double pulsed laser with a time between the pulses of 1/2500 s was used; a high-speed camera recorded every pulse separately every 1/5 s. In contrast, the recording time for the BTV was set to 3.75 min and four frames with a time between the images of 1/1600 s are recorded every 1/50 s. The hold processor (Ziegenhein and Lucas, 2015) is used for both methods in order to overcome the sampling bias.

The PDFs of v' for case 13, which are shown in Fig. 9, are in good agreement. At zero fluctuations near the wall between 0.0375 m $< x <$ 0.05 m, however, the results are slightly different but difficult to compare since the BTV graph is too noisy here. Nevertheless, the peak at around -0.12 m/s is clearly represented by both measuring techniques. The PDFs of the fluctuation towards the center at 0.0875 m $< x <$ 0.1 m are almost perfectly matching.

The time averaged liquid velocity profiles that are obtained with PIV and BTV are perfectly matching until case 13 as shown in Fig. 10. Nevertheless, for case 13 and 20 the results obtained with PIV are still in good agreement although the laser sheet is disturbed by the bubbles distinctly.

The results for $v'v'$ and $u'u'$, which are shown in Fig. 11 a), are similar up to case 20. Nevertheless, some deviations occur. For case 3 the peak of the $v'v'$ graph obtained with BTV is closer to the wall than the peak obtained with PIV. In fact, the amount of the naturally occurring micro bubbles is very low for this case because of the small gas volume flow rate. In combination with the small void fraction in general, the PIV technique might be favorable for case 3. For case 4 and case 5, however, the obtained Reynolds stresses are very similar.

Since the resolution of the high-speed camera used for the BTV measurements is limited, two measurements were needed to evaluate half of the column. At the connection of these, possible outliers at around X=0.055 m occur in the $v'v'$ profile for Case 7 and $u'u'$ profile for Case 20. Sometimes, the bubble plume tends to prefer one side of the bubble column and is swinging not symmetrical for a distinct time, which might be in combination with the two measuring areas the reason for these possible outliers. For the PIV measurements, in contrast, a larger measuring time was used and the complete measuring area was recorded at once so that such problems not arise.

The first distinct differences between the PIV and BTV measurements occur for Case 13. In the center, the normal Reynolds stresses $v'v'$ that are obtained with PIV are smaller. As mentioned above, the higher gas volume fraction for Case 13 might distort the PIV measurements; besides the bubble plume in the center, bubble

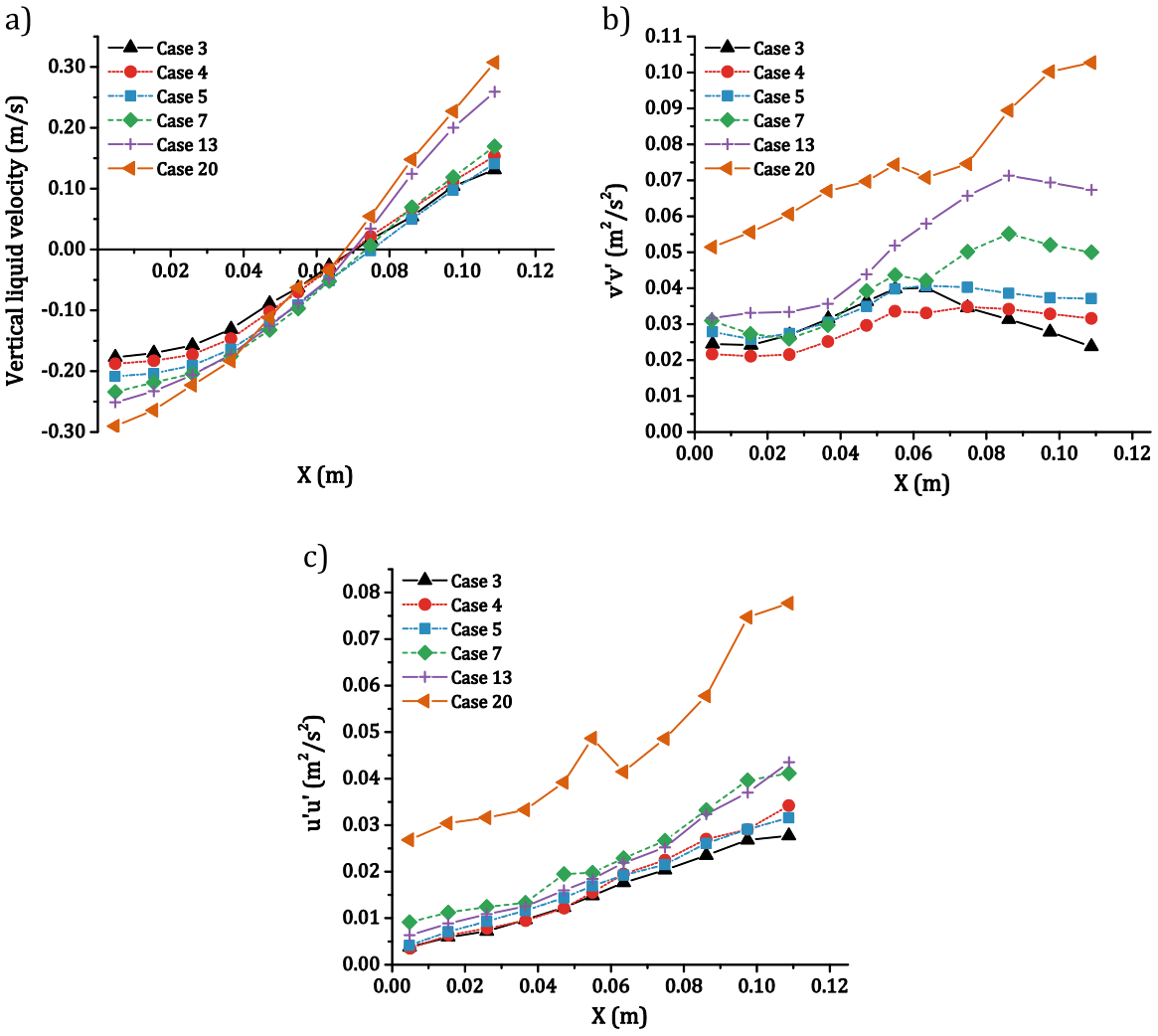

Fig. 8. Results of the particle tracking velocimetry using micro bubbles for all cases. a) Vertical liquid velocity v, b) normal Reynolds stress $v'v'$, c) normal Reynolds stress $u'u'$ (u is the horizontal liquid velocity).

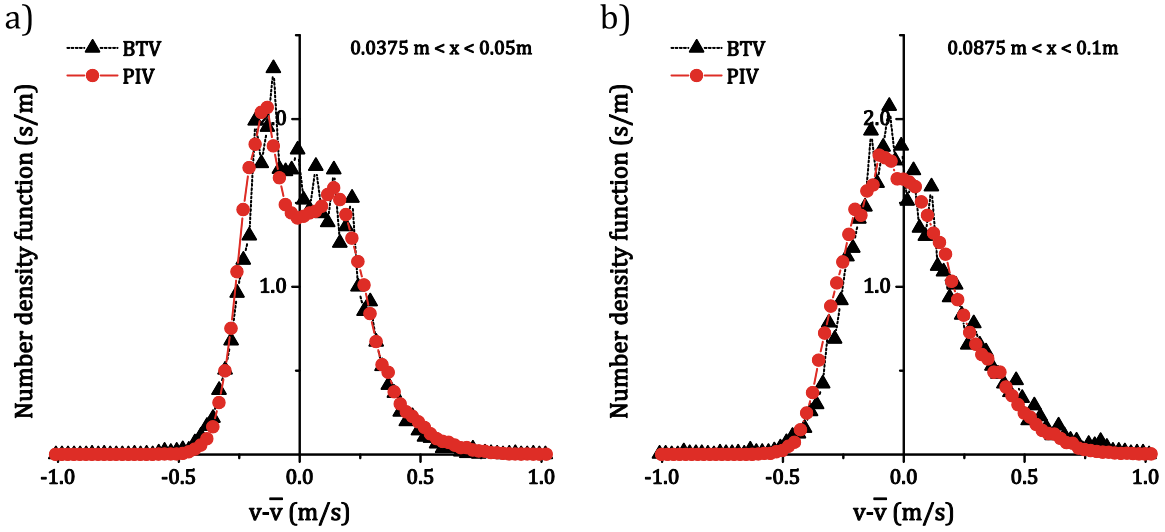

Fig. 9. The PDFs of v' that are obtained with PIV and BTV for case 13. a) Near the wall between 0.0375 m $< x <$ 0.05 m, b) towards the center between 0.0875 m $< x <$ 0.1 m.

clusters that are pulled downward near the walls block the laser assembled at the side of the bubble column. In comparison, the BTV measurements are easier to evaluate for case 13 since the amount of micro bubbles is increasing with increasing volume flow rate. In addition, the volume illumination is not as strong disturbed by the higher gas void fraction. Nevertheless, the results are still in good agreement as also discussed above by using the PDFs of the fluctuation shown in Fig. 9.

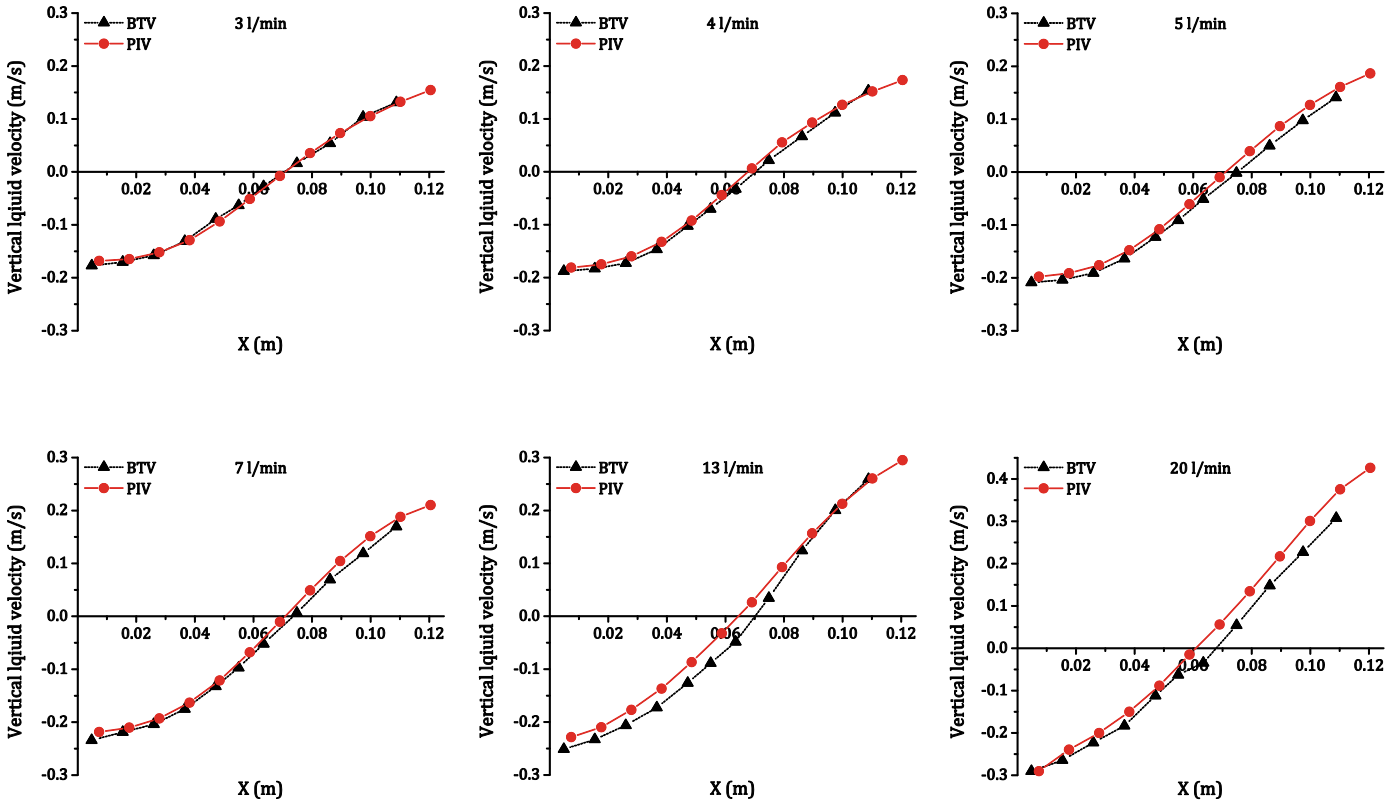

Fig. 10. The vertical liquid velocity for different gas volume flow rates.

A mismatch between both methods is obtained for case 20; all sizes of bubbles are pulled downward by the circulating flow so that the light sheet of the PIV laser is barely available. In contrast, the BTV measurements are still good manageable because of the volume illumination. Although the agreement is good for the time-averaged velocity, the normal Reynolds stresses obtained with PIV are strongly under predicted. These normal Reynolds stresses are in the range of the results obtained for case 13, which is not reasonable. As expected, the results for case 20 obtained with BTV are higher than the results for case 13. Therefore, for case 20 the BTV results are more reasonable than the PIV results.

The results for the cross Reynolds stress component $u'v'$ are shown in Fig. 11 b). Similarities to the normal components are observed so that only the results for case 3, 7 and 13 are shown. The agreement between both measuring techniques is acceptable. However, the shorter measuring time in combination with a relatively small amount of micro bubbles might lead to an insufficient statistic in the BTV measurements, especially for case 3. Surprisingly, for case 13 the graphs are matching almost perfectly.

5. Discussion

The particle relaxation time of the micro bubbles is comparable to other measurement techniques used in multiphase flows. Different micro bubble sizes are compared to each other in order to investigate their capability to follow the flow; bubbles in the range of 150–300 μm are found to represent the flow well for the present setup. Although this range has to be determined for every application explicitly, it is a good starting point for buoyancy driven bubbly flows. To be certain the Stokes number should be used, but the characteristic time scale of complex bubbly flows is not assessable with present models.

Nevertheless, considering a steady state homogenous buoyancy driven bubbly flow like that reported by Juliá et al. (2007) the energy dissipation can be estimated by calculating the energy input. The energy input per mass liquid per time, $\dot{e}$, can be estimated by multiplying the drag force with the gas velocity

$$\dot{e}=\frac{3}{4}\frac{1}{d}\alpha_G C_D u_{rel}^2 u_G \approx \frac{3}{8}\sqrt{\frac{\rho g}{\sigma}}u_{rel}^2\alpha_G u_G. \tag{5-1}$$

The drag coefficient C_D is calculated using the drag law of Ishii and Zuber (1979) to $C_D=0.5d(\rho g/\sigma)^{0.5}$ for which the relative velocity u_{rel} is approximately 0.22 m/s neglecting swarm effects. From the experiments $\alpha_G=0.076$ and $u_G\approx u_L+u_{rel}=0.24$ m/s so that $\dot{e}=0.122$J/(kg s). Assuming that the energy dissipation due to drag at the walls is negligible, the turbulent energy dissipation ϵ is equal $\dot{e}$. Using the Stokes time scale $\tau_n=(\nu/\epsilon)^{0.5}=2.8$ms, the Stokes number of 100 μm bubbles and 300 μm bubbles would be 0.11 and 0.9 respectively.

Measuring the turbulent energy dissipation is difficult in general; nevertheless, to get an idea for the dissipation in turbulent bubbly pipe flow the measurements of Liu (1989) are used. A 38.1 mm diameter pipe with a Reynolds number of 14,000 and a gas load of approximately 5 percentage was used. The energy dissipation was determined to 0.3J/(kg s) near the wall so that the Stokes number is similar to the above discussed homogenous bubble column. Looking at the present case and taking the distance between the two plates (50 mm) as characteristic length and the characteristic velocity to 0.2 to 0.4 m/s (the averaged velocity in the center) a Reynolds number between 10,000 and 20,000 is obtained, which might be comparable to the discussed pipe flow. The production of turbulent kinetic energy and dissipation of such, however, might be spatially divided due to the partial gassing so that an estimation of ϵ for the present case is difficult.

Certainly, micro bubbles of finite sizes will perhaps never behave like perfect tracer particles due to their density difference (Volk, et al., 2008). In general, due to the slip velocity the fluid near the lighter micro bubbles is constantly changing so that velocity

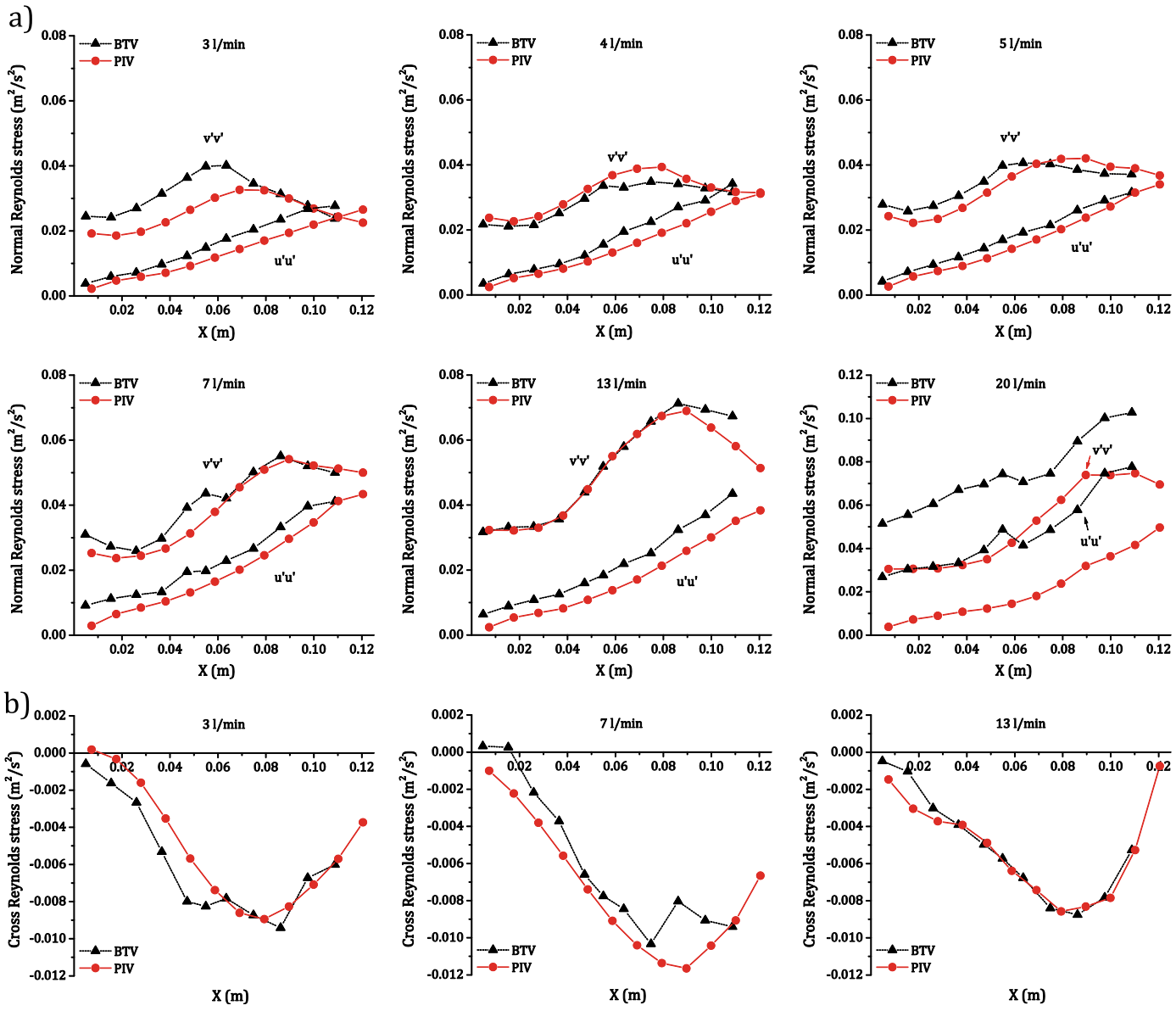

Fig. 11. Reynolds stress components obtained by using PIV and BTV. a) Normal Reynolds stress components $v'v'$ and $u'u'$ (u is the horizontal liquid velocity), b) cross Reynolds stress component $u'v'$.

correlations along the track drops more rapidly, which is known as the crossing trajectories effect (Yudine, 1959) (Csanady 1963). An advantage of the density difference is that the particle time scale of the micro bubbles is smaller compared to solid particles with equal size so that by comparison larger micro bubbles can be used for tracking, which reduce the measuring effort distinctly. On the other hand, such larger micro bubbles could be easily larger than the Kolmogorov length $\eta = \left(\nu^3/\epsilon\right)^{0.25}$, which might result in complex flow-particle interactions (Xu and Bodenschatz, 2008) (Bourgoin et al., 2011). Indeed the Kolmogorov length of the above discussed examples is approximately 50μm, which is distinctly smaller than the micro bubble sizes used in the present study.

Despite of their reasonable Stokes number, it becomes clear that large micro bubbles like those that are used in the present study are not suitable to study turbulent structures of a flow deeply. Nevertheless, the averaged liquid velocity and turbulent kinetic energy, which are usually determined by the large scales of a flow, can be reliable determined as shown in the present work. In combination with the very low-effort of tracking the larger micro bubbles, the completely non-invasive behavior of micro bubbles and that the system creates the tracking particles itself, a valuable technique is obtained for bubbly flows.

6. Conclusion

In the present work, tracking single micro bubbles is combined with a volume illumination and applied to bubbly flows. The micro bubbles are identified in a narrow measuring volume by using a narrow depth of field camera setup in combination with an edge filtering technique. The results obtained with this method are compared to PIV measurements that were used in the past at low superficial gas velocities in bubbly flows frequently. The agreement at such low superficial gas velocities is excellent when enough micro bubbles are present in the flow. Increasing the gas flow rate, a point is reached at which PIV cannot produce meaningful results anymore whereas, because of the volume illumination, micro bubbles can still be tracked without problems.

Using micro bubbles as tracer has due to their density difference some disadvantages that have to be taken into account as

discussed in the text. The benefit of micro bubbles, however, is that they do not contaminate the flow like conventional extrinsic tracers, which is in almost every multiphase flow essential to obtain reproducible results. Another comfortable benefit is that in most flows micro bubbles are generated by the system itself so that no seeding is necessary. Certainly, micro bubbles can also be generated artificially using different methods, which might be necessary for some flow conditions as discussed in the text.

Using the volume illumination technique, relatively high superficial gas velocities are manageable in comparison to the light sheet technique used for PIV measurements. Nevertheless, the depth of field and the screening out of blurred particles need to be calibrated beforehand. With test prints on glass the depth of the measuring volume was determined to below 2 mm in the present work. Despite the better characteristics of the volume illumination in bubbly flows, the previously described sampling bias found for PIV measurements with a light sheet (Ziegenhein and Lucas, 2015) is also present. This sampling bias might be found for measuring techniques observing bubbly flows from the outside in general. For the present setup, the hold processor used to overcome this error for PIV measurements (Ziegenhein and Lucas, 2015) gives reasonable results.

From an engineering point of view, the described simple and cheap technique is a possible candidate for reliable measurements in dense bubbly flows as well as in difficult to access problems like pilot plants or submerged oceanic multiphase flow problems. In combination with naturally occurring micro bubbles, even no seeding of the flow with additional tracers is needed so that a truly non-invasive method is gained.

Acknowledgments

This work was funded by the Helmholtz Association within the frame of the Helmholtz Energy Alliance “Energy Efficient Chemical Multiphase Processes” (HA-E-0004).

References

Bourgoin, M., et al., 2011. Turbulent transport of finite sized material particles. J. Phys.: Conf. Ser. 318, 1–10.
Bozzano, G., Dente, M., 2001. Shape and terminal velocity of single bubble motion: a novel approach. Comput. Chem. Eng. 25, 571–576.
Calzavarini, E., Cencini, M., Lohse, D., Toschi, F., 2008. Quantifying turbulence-induced segregation of inertial particles. Phys. Rev. Lett. 101, 1–5 (August).
Canny, J., 1986. Computational approach to edge detection. IEEE Trans. Pattern Anal. Mach. Intell. 8 (6), 679–698.
Csanady, G.T., 1963. Turbulent diffusion of heavy particles in the atmosphere. J. Atmos. Sci. 20, 201–208.
Deen, N., Solberg, T., Hjertager, B., 2001. Large eddy simulation of the gas–liquid flow in a square cross-sectioned bubble column. Chem. Eng. Sci. 56, 6341–6349.
Feng, Y., Goree, J., Liu, B., 2011. Errors in particle tracking velocimetry with high-speed cameras. Rev. Sci. Instrum. 82, 053707-1–053707-7.
Fish, F.E., Legac, P., Williams, T.M., Wei, T., 2014. Measurement of hydrodynamic force generation by swimming dolphins using bubble DPIV. J. Exp. Biol. 217 (2), 252–260.
Graff, E.C., Pereira, F., Gharib, M., 2008. Defocusing digital particle image velocimetry: a volumetric dpiv technique for dual and single phase flows. In: Proceedings of the 14th International Symposium on Applications of Laser Techniques to Fluid Mechanics. Lisbon, Portugal, pp. 1–12.
Ishii, M., Zuber, N., 1979. Drag coefficient and relative velocity in bubbly, droplet or particulate flows. AlChE J. 25, 843.
Ishikawa, M., Irabu, K., Teruya, I., Nitta, M., 2009. PIV measurement of a contraction flow using micro-bubble tracer. J. Phys.: Conf. Ser. 147, 012010.
Juliá, J.E., Hernandez, L., Chiva, S., Vela, A., 2007. Hydrodynamic characterization of a needle sparger rectangular bubble column: Homogeneous flow, static bubble plume and oscillating bubble plume. Chem. Eng. Sci. 62 (22), 6361–6377.
Liu, T.T.-J., 1989. Experimental investigation of turbulence structure in two-phase bubbly flow (Ph.D. thesis). Northwestern University, Evanston, Illinois.
Luo, H.-P., Al-Dahhan, M.H., 2008. Local characteristics of hydrodynamics in draft tube airlift bioreactor. Chem. Eng. Sci. 63 (11), 3057–3068.
Ma, T., et al., 2015. Scale-adaptive simulation of a square cross-sectional bubble column. Chem. Eng. Sci. 131, 101–108.
Masood, R., Rauh, C., Delgado, A., 2014. CFD simulation of bubble column flows: an explicit algebraic Reynolds stress model approach. Int. J. Multiph. Flow. 66 (0), 11–25.
Mudde, R.F., Lee, D.J., Reese, J., Fan, L.-S., 1997. Role of coherent structures on reynolds stresses in a 2-D bubble column. Part. Technol. Fluid. 43 (4), 913–926.
Murai, Y., Oshi, Y., Takeda, Y., Yammamoto, F., 2006. Turbulent shear stress profiles in a bubbly channel flow assessed by particle tracking velocimetry. Exp. Fluids 41, 343–352.
Ryu, Y., Chang, K.-A., Lim, H.-J., 2005. Use of bubble image velocimetry for measurement of plunging wave impinging on structure and associated greenwater. Meas. Sci. Technol. 16, 1945–1953.
Simiano, M., et al., 2006. Comprehensive experimental investigation of the hydrodynamics of large-scale, 3D, oscillating bubble plumes. Int. J. Multiph. Flow. 32, 1160–1181.
Volk, R., et al., 2008. Acceleration of heavy and light particles in turbulence: comparison between experiments and direct numerical simulations. Phys. D: Nonlinear Phenom. 237 (14–17), 2084–2089.
Xu, H., Bodenschatz, E., 2008. Motion of inertial particles with size larger than Kolmogorov scale in turbulent flows. Phys. D: Nonlinear Phenom. 237 (14–17), 2095–2100.
Yudine, M.I., 1959. Atmospheric diffusion and air pollution. Adv. Geophys. 6, 185–191.
Ziegenhein, T., Lucas, D., 2016. On sampling bias in multiphase flows: particle image velocimetry in bubbly flows. Flow. Meas. Instrum. 48, 36-31.
Ziegenhein, T., Rzehak, R., Lucas, D., 2015. Transient simulation for large scale flow in bubble columns. Chem. Eng. Sci. 122, 1–13.